JOURNAL OF THE KOREAN ASTRONOMICAL SOCIETY
30: 95 ~ 106, 1997

VELOCITY DISTRIBUTION OF DARK MATTER GALACTIC HALO

OH, K.S.
Department of Astronomy and Space Science
Chungnam National University, Daejeon, Korea
(Received Feb. 12, 1997; Accepted Mar. 28, 1997)

ABSTRACT

We investigate the velocity distribution of dark matter in the disk of a galaxy like the Milky Way at the solar radius. Using N-body simulations with the total mass and z-component of angular momentum conserved, we calculate the response of a dissipationless dark matter galactic halo during the dissipational collapse of the baryonic matter in spiral galaxy formation. The initial distribution of dark matter and baryonic particles is assumed to be a homogeneous mixture based on a King model. The baryonic matter is assumed to contract, forming the final luminous components of the galaxy, namely the disk and, in some cases, a bulge and central point. Both slow and fast growth of the luminous components are considered. We find that the velocity distribution of dark matter particles in a reference frame rotating slowly about the galaxy center in the plane of the disk is similar to a Maxwellian, but it is somewhat boxier, being flatter at the peak and truncated in the tails of the distribution. We tabulate parameters for the best-fitting Maxwellian and modified-Maxwellian distributions. There is no significant difference between slow collapse and fast collapse for all these results. We were unable to detect any effect of disk formation on the z-dependence of the dark matter density distribution.

I. INTRODUCTION

Fairly flat rotation curves are a well known feature of spiral galaxies (Bosma 1978, Rubin *et al.* 1980, 1982, 1985; for recent data and references cf. also Casertano & van Gorkom 1991). For the rotation curve to remain flat beyond the optical radius requires a massive dark halo with density falling off roughly as R^{-2}.

Fall & Efstathiou (1980) assumed that most matter is dark and dissipationless and that the material destined to form the luminous parts of galaxies collapsed dissipatively after the dark material reached dynamical equilibrium. After the density of the disk is specified from the rotation velocity of the disk, they found the density profile of the halo from the above assumptions.

An improved scheme was adopted by Blumenthal *et al.* (1986). They used an analytic approach and N-body simulations. In the analytic calculation they investigated various baryonic mass fractions and disk scale lengths, and found that baryonic mass fraction of roughly 0.1 and disk scale length of roughly 0.07 (in units of the initial truncation radius) gave a flat rotation curve. In the N-body simulation they used an initially well-mixed system of baryonic and dark particles. The baryonic particles were merged together when they approached within a certain distance, producing a new particle having the sum of the masses and the velocity of the center of mass of the previous two particles. The N-body result also showed a flat rotation curve. At nearly the same time Barnes (1987) also made N-body simulations with King model. He also found relatively flat rotation curves. He concluded that if the initial halo core radius is chosen too small, it is easy to get a falling rotation curve.

Blumenthal *et al.* and Barnes used an assumed predetermined profile for the halo, whereas Ryden & Gunn (1987) adopted a more self-consistent halo. They started with the perturbation spectrum of cold dark matter (CDM) and calculated the rms angular momentum acquired by a particle bound to a density maximum. Then they grew a halo of dark matter by adding successive mass shells with known binding energy and angular momentum to the previously collapsed mass distribution. As the baryonic fraction of the mass dissipated and fell to the center, the dark matter

was drawn inward after it. If the adiabatic invariants of the dark halo are conserved, the halo is compressed in such a way that the resulting rotation curve is flat over a large range of radii.

Several attempts have been made to find the distribution of the dark matter halo in protogalaxies (Frenk *et al.* 1985; Hoffman 1988; Quinn *et al.* 1986).

There are several weak assumptions in each of the above works; no reaction of halo during the dissipational collapse of baryonic matter (Fall & Efstathiou 1980), arbitrary boundary of isothermal sphere (Blumenthal *et al.* 1986), adiabatic approximation for the dark matter profiles (Blumenthal *et al.* 1986, Ryden & Gunn 1987, Blumenthal 1988), and lack of conservation of total mass of the system (Barnes 1987). In this paper we have tried to improve on some of these shortcomings. We use a King model which has very large core radius, so that it mimics an isothermal sphere in the inner region. The baryonic and dark matter particles are initially well mixed, so that each particle is a mixture of dark matter and baryonic matter. We reduce the mass of the baryonic matter in each particle, and this mass goes into the central region, where we grow a baryonic disk and spheroid. Therefore the total mass of the system is conserved. After the dissipational collapse, we calculate the angular momentum of the disk with the various disk scale lengths from the squeezed dark halo, assuming that the response of halo is not sensitive to the disk scale length. Then we choose the disk scale length which conserves angular momentum. This new disk scale length is used for the next run. From this process we achieve a self-consistent disk scale length. It turns out two iterations are enough to conserve the initial angular momentum of the baryonic matter.

Realistic dissipational collapse of baryonic matter was simulated by Katz & Gunn (1991). They used TREESPH code which calculates the gravitational forces with hierarchical tree algorithm, and determine the gasdynamic properties by smoothed particle hydrodynamics. The code can include the dissipational effect by allowing the gas to cool radiatively. Combining dark matter and baryonic matter in 10 to 1 ratio, and assuming a power-law slope in cold dark matter scheme, they could mimic the spiral galaxy of thin disk of gas and a dark matter halo. The rotation curve also resembles that of real galaxies. They also found that the inner disk transfer more than 50% of its original angular momentum to the dark halo.

None of the above authors reported the velocity distribution of dark matter particles. The main purpose of this paper is to calculate how disk formation affects the velocity distribution of dark matter particles. We consider especially the dark matter in the vicinity of the disk, at intermediate galactocentric radii like that of the sun. We find that the Maxwellian distribution in the absence of a disk is somewhat modified, especially for the tangential velocities in the plane of the disk. These results could provide useful information for dark matter detection, in particular for predicting the annual modulation effect, as discussed by Drukier, Freese, & Spergel (1986), by Freese, Frieman, & Gould (1988), and in the review articles by Primack, Seckel, & Sadoulet (1988) and Smith & Lewin (1990).

In section 2 we describe the general numerical scheme, initial conditions, and model parameters. The results of the simulations are in section 3. We summarize our results in section 4.

II. DESCRIPTION

(a) Equations of Motion

We use the standard exponential thin disk potential (Freeman 1970), originally developed by Toomre (1963). We can solve the Laplace equation for this disk with the method of separation of variables and combine it with Gauss' theorem in the plane of the disk to represent the potential in terms a Bessel integral :

$$\phi(r,z) = 2\pi G \int_0^\infty J_o(rk) S(k) e^{-k|z|} dk, \tag{1}$$

where G is the gravitational constant, $r = (x^2 + y^2)^{1/2}$ is the distance from the z-axis, J_o is the first kind of Bessel function of order zero, and

$$S(k) = \int_0^\infty J_o(ku) u \mu(u) du, \tag{2}$$

where $\mu(u)$ is the surface density at $u = (x^2 + y^2)^{1/2}$. Consider an infinitely thin disk whose surface density is given by

$$\mu(r) = \mu_o \exp(-\alpha r), \tag{3}$$

where the normalization constant is

$$\mu_o = \frac{M_d \alpha^2}{2\pi}, \tag{4}$$

where $\alpha = S_d^{-1}$ is the inverse of the disk scale length, and M_d is the total mass of the disk. For this exponential disk

$$S(k) = \frac{\mu_o \alpha}{(\alpha^2 + k^2)^{3/2}}, \tag{5}$$

so that

$$\phi(r, z) = 2\pi G \mu_o \alpha \int_0^\infty dk J_o(rk) T(k, z), \tag{6}$$

where

$$T(k, z) = \frac{e^{-k|z|}}{(\alpha^2 + k^2)^{3/2}}. \tag{7}$$

The particle accelerations are obtained by differentiating the potential to obtain

$$F_r = -\left(\frac{\partial \phi}{\partial r}\right) = 2\pi G \mu_o \alpha \int_0^\infty dk J_1(rk) k T(k, z), \tag{8}$$

$$F_z = -\left(\frac{\partial \phi}{\partial z}\right)_{z \neq 0} = 2\pi G \mu_o \alpha \, \mathrm{sign}(z) \int_0^\infty dk J_o(rk) k T(k, z), \tag{9}$$

where F_r and F_z are the accelerations parallel and perpendicular to the plane of disk respectively. $F_z = 0$ at $z = 0$ because of the symmetric mass distribution in the z-direction. To efficiently compute the force and acceleration, we make a table with a grid in r and z. Using this table, we interpolate or extrapolate to obtain the acceleration. The accelerations for different disk scale lengths are easily obtained from the table by appropriate scaling.

Because of the thin disk approximation, the force is discontinuous across the disk plane, which causes numerical difficulty in our code. This problem can be solved by introducing a softening parameter, which we take here to be a multiplicative factor $|z|^3/(z^2 + \varepsilon^2)^{3/2}$ applied to the force, F_z, where ε is the softening parameter. This scheme was also used by Barnes & White (1984). One nice feature of this approach is that it mimics the effect of an exponential density distribution in the z-direction. The approximation is particularly good when the density scale height is much smaller than the disk scale length such as in our Galaxy.

Table 1. MOEDL PARAMETERS

(1)	W_o (2)	c (3)	r_c/R_t (4)	λ (5)	$(S_d/R_t)_{ad}$ (6)	S_d/R_t (7)	τ_g/τ_c (8)	Final Components (9)
Model A	0.5	1.321	0.757	0.07	0.040	0.0370	10	Disk, halo
Model B	0.5	1.321	0.757	0.00	0.040	0.0370	10	Disk, halo
Model C	0.5	1.321	0.757	0.07	0.040	0.0375	10	Central point, bulge, disk, halo
Model D	2.0	3.195	0.313	0.07	0.058	0.0330	10	Central point, bulge, disk, halo
Model E	0.5	1.321	0.757	0.05	0.026	0.0250	10	Central point, bulge, disk, halo
Model F	0.5	1.321	0.757	0.07	0.040	0.0370	1	Disk, halo

Note ; The relative mass ratios of central point, bulge, and disk are 0.1578, 0.0388, and 0.8034, respectively.

A common choice for the distribution of matter in a protogalaxy is the isothermal sphere (e.g. Blumenthal *et al.* 1986), since it gives a flat rotation curve, but it has no outer limit and therefore has infinite mass. To limit the outer region, we adopt a King model (King 1966). The King model has very similar profile to an isothermal distribution in the inner region, but it has finite size. The real galaxy might not reach equilibrium before the dissipation of baryonic matter occurs (Quinn & Zurek 1988) because the cooling time is much less than a dynamical time in the inner regions. If this is true, then a King model is not appropriate. Nevertheless the King model is one plausible choice and is especially easy to handle.

Some of our models also include a baryonic luminous spheroid, which we model using a de Vaucouleurs profile. The potential and acceleration are numerically tabulated by Young (1976).

(b) Numerical Code

We used Aarseth's code(Aarseth 1985), which uses a force-polynomial predictor and the Ahmad-Cohen integration scheme along with a softened potential to suppress two-body relaxation. We made several runs to determine the size of the softening parameter. One easy way to test two-body relaxation is to use particles with different masses. We use two mass components, with the heavy one having twice the mass of the light one. Then we calculate the mean inter-particle distance inside 10 % of the total radius after the collapse of the baryonic matter. This distance is used as the size of the softening parameter in the next run. With this softening parameter, which is 3.3 % of the size of the system, the distributions of heavy and light particles agree well until late times within the statistical scatter.

(c) Initial Conditions

We investigated two King models. In the first case, the concentration parameter c (the ratio of tidal radius to core radius) was 1.321 (case 1), which corresponds to $W_o = 0.5$, where W_o is the central potential in units of the central velocity dispersion. In the other case, the concentration parameter was 3.195 (case 2) for which $W_o = 2.0$. The ratios of half mass radius to core radius are 0.46 for the case 1 and 0.97 for the case 2. Case 2 has more a centrally condensed core than case 1.

The initial rotation was represented by the galaxy angular momentum parameter (Peebles 1971),

$$\lambda = JE^{1/2}/GM^{5/2}. \tag{10}$$

We assumed solid body rotation with $\lambda = 0.07$ (Peebles 1971, Efstathiou & Jones 1979, Aarseth & Fall 1980) and $\lambda = 0.05$ (Barnes & Efstathiou 1987, Quinn & Zurek 1988).

(d) Parameters

We assumed no transfer of angular momentum between dark and luminous matter and took the mass fraction of baryonic matter to be 0.1 (Blumenthal *et al.* 1986). Assuming the adiabatic approximation gives the relationship between λ and α for two King models. We first made an initial guess of disk scale length $S_d = \alpha^{-1}$ from this relationship. For a given λ, a run was made with this scale length. Then we calculated the angular momentum with the new distribution of the dark matter halo for various disk scale lengths, assuming that the halo profile does not change much for slight changes in disk scale length. A second run, done with an improved disk scale length, shows very good conservation of angular momentum.

There are two well known mass models of the Galaxy, by Caldwell & Ostriker (1981) and Bahcall *et al.* (1980, 1982, 1983). Caldwell & Ostriker chose three components: an exponential disk, a Hubble law ($\sim R^{-3}$) spheroid, and a pseudo-isothermal halo. They used 14 observational constraints to determine the free parameters by minimizing the chi-squared statistics. Bahcall *et al.* used four components for the Galaxy mass distribution: a central point-mass, a de Vaucouleurs spheroid (hereafter bulge), an exponential disk, and a dark halo. They chose the shape of the central "point-mass" from 2.2 μm observations of the Galactic center by Becklin & Neugebauer (1968) and star count data for the disk and the bulge, and the observed rotation velocity to constrain the dark matter density, which they took to vary asymptotically as $R^{-1.8}$. Both models produce very similar rotation curves.

For our models which have a disk only for the baryonic component, we used the scale length and scale height of the disk in the model of Bahcall *et al.* For our three-component models (models C-E in §2.5) we also adopted the

mass model of Bahcall *et al.* because it is easier to handle numerically. In these models the distance to the Galactic center, R_o, is 8 kpc, the exponential disk scale length is 3.5 kpc, the disk scale height is 325 pc, and the effective length of the de Vaucouleurs spheroid is $R_o/3$ (de Vaucouleurs 1977, de Vaucouleurs & Buta 1978). The central point mass was limited within 1 kpc. We set the ratio of disk scale height to disk scale length to 1/11, and the effective radius of the de Vaucouleurs spheroid to be 9/11 of the disk scale length. To mimic the central point-mass we use the softened potential $(R^4 + \varepsilon^4)^{-1/4}$, with $\varepsilon \sim 0.127$ times the disk scale length. We use the Bahcall *et al.* values of mass ratios of the luminous matter components in our models C-E. The fractional mass ratios for the central point, bulge, and exponential disk are 0.1578, 0.0388, 0.8034, and total baryonic mass fraction is 0.1.

(e) Model Parameters

Units are such that $G = 1$, the total mass, $M_t = 1$, and the total size of the galaxy, $R_t = 1$. The mass of baryonic matter is 10% of the total mass and the rest is dark matter. Our approach is to generate 2000 particles randomly from the King distribution and scale the velocities such that the original systems are virialized. For rotating galaxies, solid body rotation for the chosen value of λ is then added. These models are thus slightly out of initial equilibrium, although they are virialized. We compared the position and velocity distributions of these data with the assumed theoretical profiles. The Kolmogorov-Smirnov test (Gibbons 1976; hereafter K-S test) shows good agreement.

We simulate several models. The parameters for simulated cases are given in Table 1. Column (4) shows the ratio of core radius r_c of the King model to the total size of the galaxy (truncation radius R_t). Column (6) is the disk scale length in terms of the total size of the galaxy. This is the first-guess scale length predicted by the adiabatic invariant approximation. Column (7) is the improved disk scale length actually used in the simulation. This disk scale length conserves the angular momentum in Model A and Model F. The growth time scale of baryonic components in terms of half mass crossing time is in column (8). Column (9) shows the mass components included in the model.

Model A, with a disk and $\lambda = 0.07$, provides a simple comparison to the adiabatic invariant prediction. Model B is the same as Model A but has $\lambda = 0$. By comparison with A, it gives an idea of how the final distribution of dark matter particles depends on their initial rotation. Model C adds a central point-mass and bulge to Model A. In Model D a different King model is used, and in Model E a different value of λ. So far we consider a slow collapse (in 10 crossing times) of baryonic matter. In Model F a fast collapse (in 1 crossing time) is considered to see the dependence on the collapse time scale of baryonic matter.

The initial angular momentum of the baryonic matter which goes into the central point source and bulge is neglected in Models C, D, and E. Therefore for these three models, the initial angular momentum of only the disk portion of the baryonic matter is conserved, with the disk scale length as shown in column (7). For the initial estimate of the disk scale length in column (6), only the dark matter halo and disk are considered to conserve angular momentum. These approximations are not crucial because we use the adiabatic calculation for the initial trial simulation and for the comparison.

III. RESULTS

We computed 12 runs in each model, and the 12 runs have the same basic initial conditions, but the initial positions and velocities are generated with a different random number seed. The masses of the final baryonic components grow linearly over 10 crossing times mimicking their dissipational collapse except in Model F, in which they grow in 1 crossing time. One crossing time corresponds $3.4 \times 10^8 (R_{100}^3/M_{12})^{1/2}$ years for $W_o = 0.5$ and $2.9 \times 10^8 (R_{100}^3/M_{12})^{1/2}$ years for $W_o = 2.0$, where M_{12} is the mass in the units of $10^{12} M_\odot$ and R_{100} is the radius in the units of 100 kpc. We stop the run after 15 crossing times in Model A through Model E due to two-body relaxation effects, but stop at 10 crossing times in Model F. One run usually takes 75 cpu hours (50 cpu hours in Model F) in a Sun 4 series computer. Runs from 11 crossing times to 15 crossing times are summed for better statistics, except in Model F, in which runs from 6 to 10 crossing times are summed. In total, there are 12 representations of the initial data, and 60 data sets for the final results. The relative error in the z-component of angular momentum of dark matter is less than 5×10^{-4} in our simulations.

(a) Rotation Curves

Rotation velocities of the initial dark matter profile, final dark matter profile, disk, central point mass, bulge, final total, and adiabatic invariant prediction are shown in Fig. 1 for Model E. The rotation curve of the dark matter halo inside 0.5 disk scale lengths is not reliable because of the small number of particles. The rotation curve of the adiabatic prediction uses a different disk scale length from the real run (see Table 1). The adiabatic calculation considered the disk and halo only. The rotation curve of adiabatic invariance uses the disk scale length predicted by adiabatic invariance and scale length of central point and bulge in the real run.

The adiabatic rotation curve is generally flatter and higher in the inner region than the real simulation except Model D. The reason why the adiabatic prediction is smaller than the real simulation in Model D is that the adiabatic invariance uses the very large disk scale length (see Table 1) which causes a small rotation value in the inner regions. The final rotation curves of dark matter are very similar among the models except Model D which uses a different King model as an initial condition. The rotation curves in the inner region are dominated by baryonic matter. The dark matter halo shrinks due to the dissipational collapse of baryonic matter. This dissipational collapse scheme gives relatively flat rotation. Comparison between Model D and the model of Bahcall *et al.* (1983) shows that there is a large difference in the halo profile only, but not in other components.

(b) Mean Velocities

We looked at the mean velocities of the initial and final sample. We chose a ring-shaped slab in the plane of disk. We first looked at samples between $0 < |z| < 0.01$ and $0.01 < |z| < 0.02$. The K-S test of these two samples shows that these two samples agree very well. Therefore we decided to use the data from $0.0 < |z| < 0.02$ to increase the number of samples to get better statistics. The width of the slab (along the radial direction) is 0.04 and thickness of slab (perpendicular to the disk plane) is 0.02 in each side of the plane. The units of these width and thickness are in unit in which the size of the galaxy is unity. These results are shown in Oh (1989).

(c) Velocity Distributions

The velocity distributions at several radii are studied. These positions are 0.05, 0.09, 0.13, and 0.27. We selected the samples from the slab of above radii. The width and thickness of these slabs are 0.04. The samples are from 60 sets of data as in the cases of mean velocity analysis. The distributions of radial velocity and transverse velocity perpendicular to the plane show that they are symmetric with respect to the inertial frame whose mean velocity is zero. Therefore we have chosen the absolute value for these two velocities. The transverse velocity on the plane has net motion due to the initial solid body rotation except in Model B. Therefore we used the positive and negative velocities of the sample. We compared these sample distributions with a Maxwellian velocity distribution. The comparison Maxwellian distribution is given by

$$f(V) = \frac{2N'}{\sqrt{2\pi}\, b} \exp\left[-\frac{V^2}{2b^2}\right], \tag{11}$$

for V_r and V_z, where b is the width of the Maxwellian and N' is the expectation value of total number of particles which gives the best fit to the sample distribution (N' is always larger than the actual number of particles). For V_θ the comparison distribution is

$$f(V) = \frac{N'}{\sqrt{2\pi}\, b} \exp\left[-\frac{(V-\bar{V})^2}{2b^2}\right], \tag{12}$$

where $\bar{V}$ is the velocity of the reference frame. We chose four different reference frames: inertial, mean velocity of sample, rotation velocity, and the frame that gives minimum chi-squared (χ^2), i.e., the best fit. We made grids in N' and b, and calculated χ^2 values in these grids. A set of parameters is determined that gives minimum χ^2. In V_θ we also need to consider a grid for $\bar{V}$ in the case of best fit. The results for Model E are shown in the Figures 2a-c. The results for other models are very similar to Model E. When the χ^2 is calculated, the bins that have less than four particles are neglected. If the number in the bin is four, then we added this number to the adjacent bin to make it greater than 4, and expanded the size of the bin. As a result we compared with a truncated Maxwellian distribution. The χ^2 values are given in Tables 2a-2f of Oh (1989)

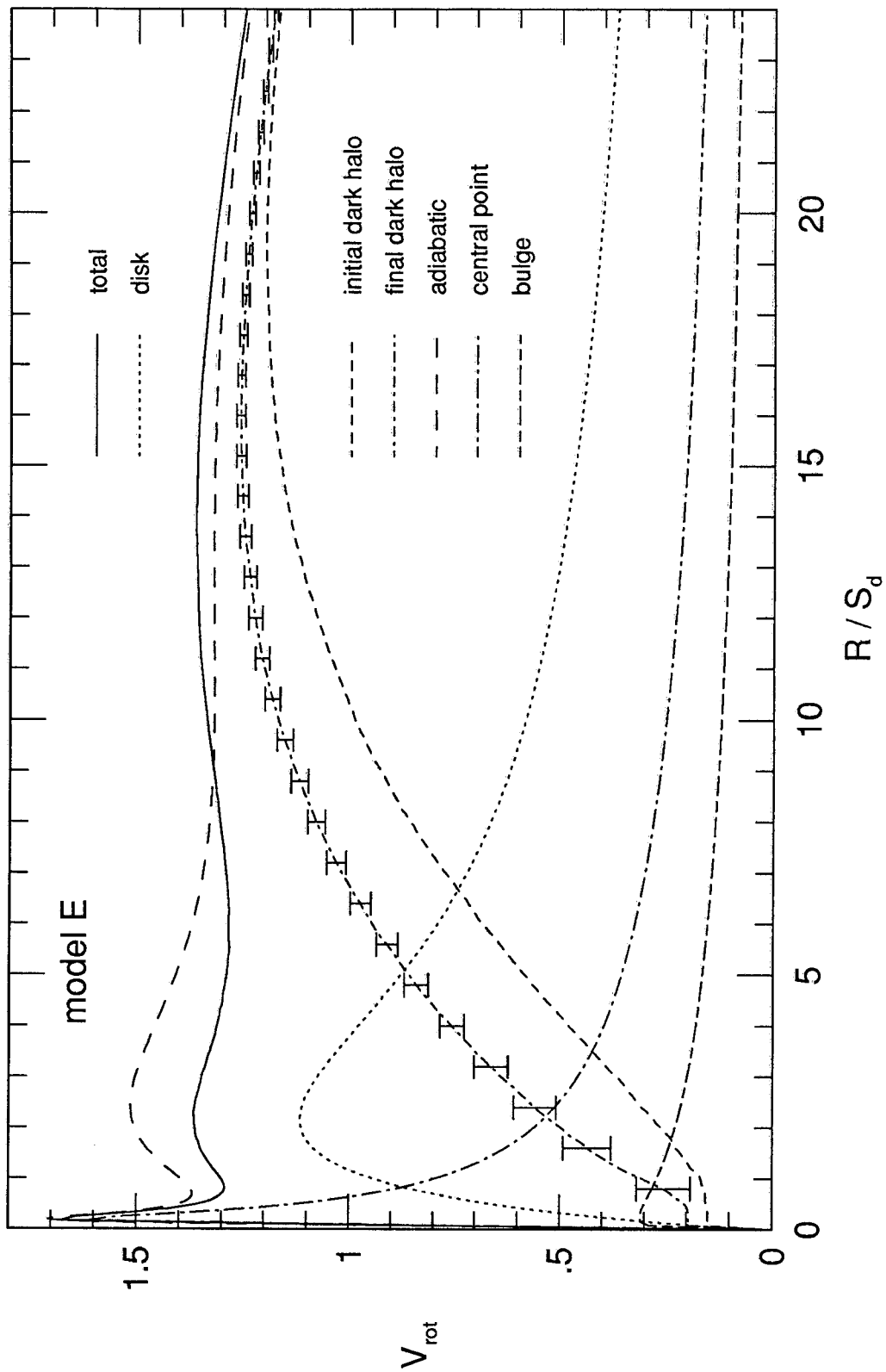

Fig. 1. Rotation curves of Model E are shown. The radius is in terms of disk scale length, and 60% of the total size is shown. Velocity is in units such that total size and total mass are unity. Unit velocity corresponds to $208 \times (M_{12}/R_{100})^{1/2}$ km/sec, where M_{12} is the mass in the units of $10^{12} M_{\odot}$ and R_{100} is the radius in the units of 100 kpc. The 1σ error bars are given in the final dark matter halo.

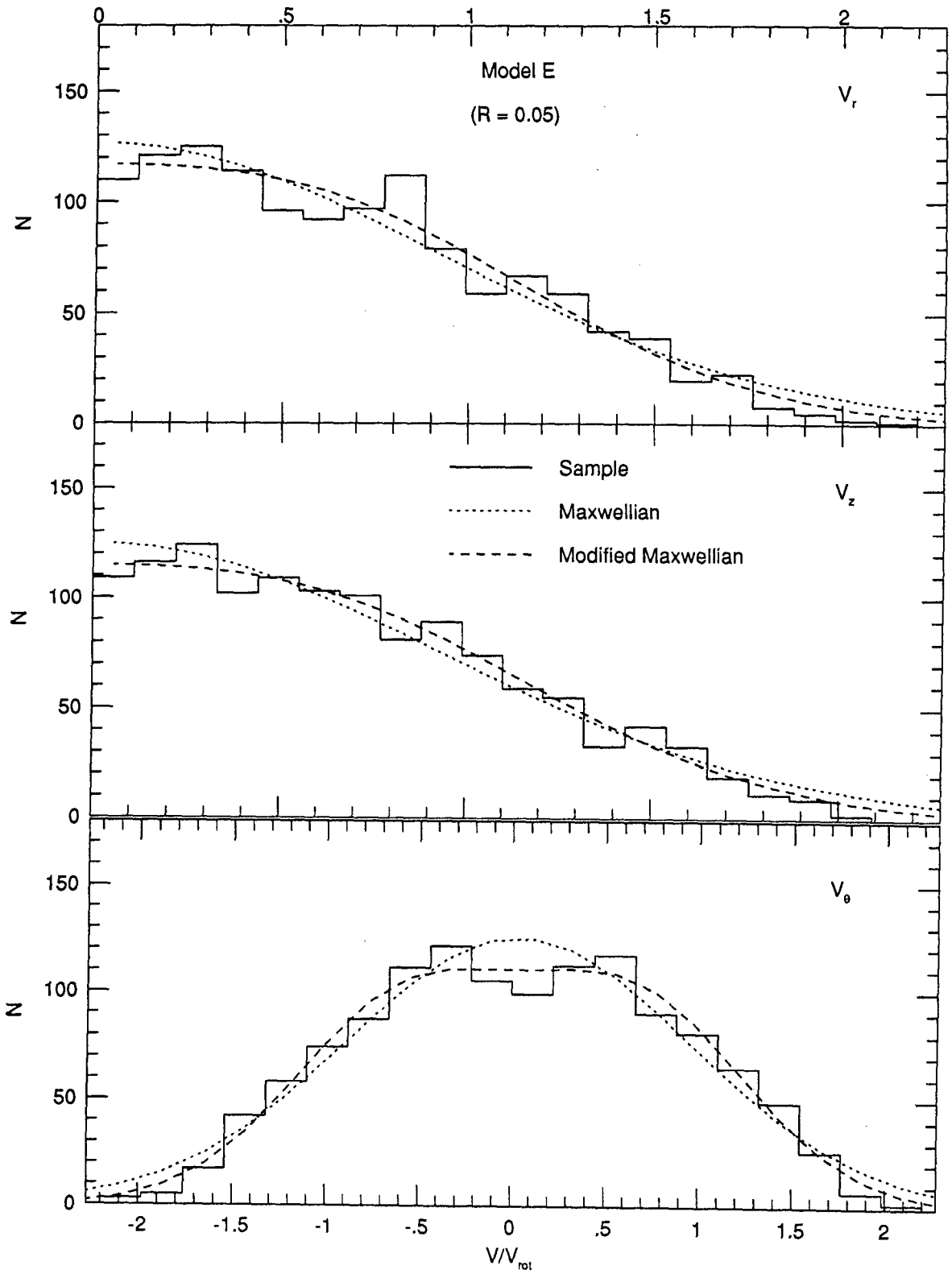

Fig. 2(a). Velocity distributions for Model E. The horizontal axis is the velocity in the units of rotation velocity. In the panels labeled V_θ, the horizontal axis is actually $V_\theta - \bar{V}_\theta$. The vertical axis is the number of samples and the expectation values of the Maxwellians. The solid lines are the sample distribution and the dotted lines are the Maxwellian distributions that give minimum χ^2. The dashed lines are the modified Maxwellian distributions that give minimum χ^2.

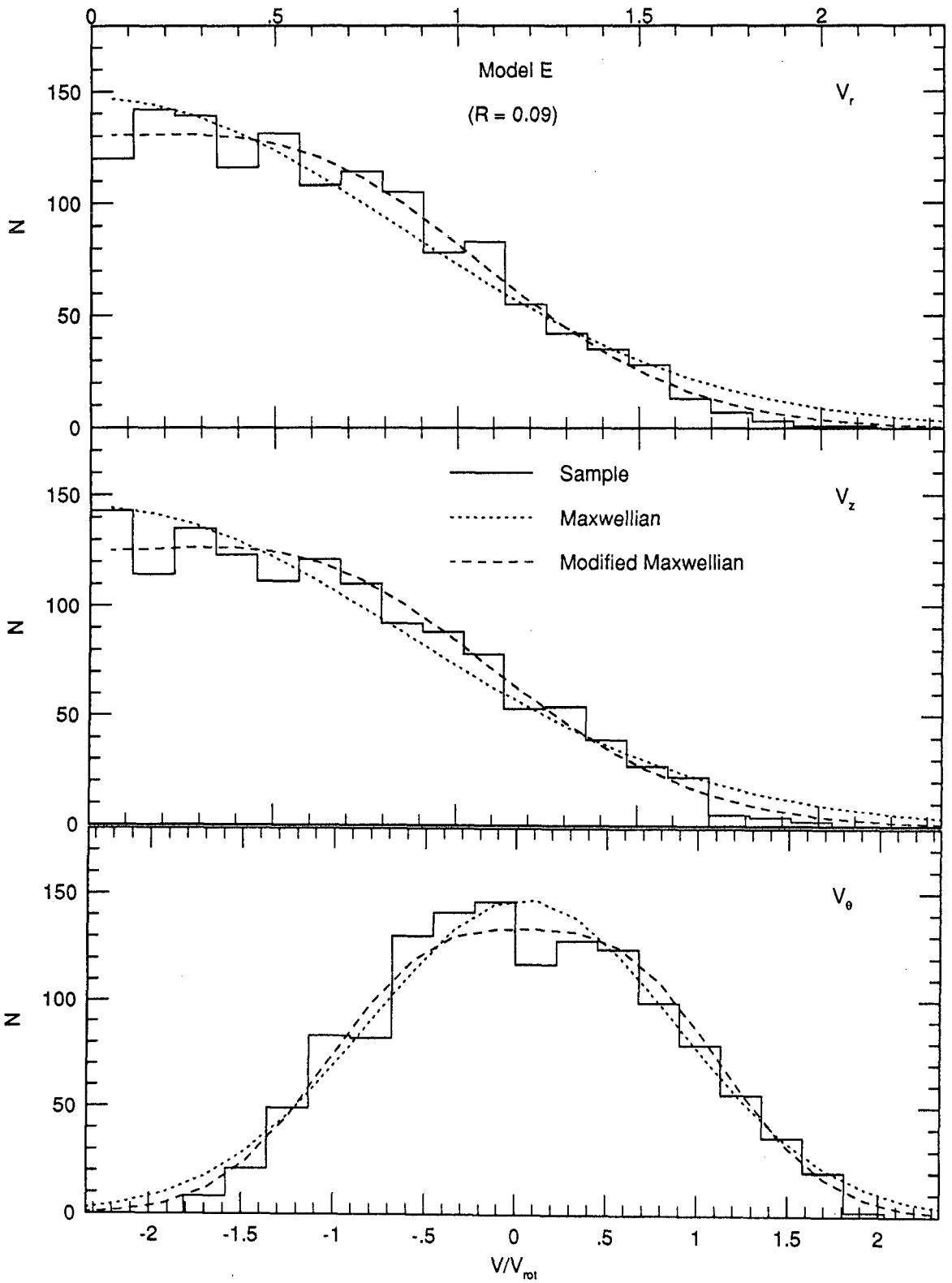

Fig. 2(b). Velocity distributions for Model E. The horizontal axis is the velocity in the units of rotation velocity. In the panels labeled V_θ, the horizontal axis is actually $V_\theta - \bar{V}_\theta$. The vertical axis is the number of samples and the expectation values of the Maxwellians. The solid lines are the sample distribution and the dotted lines are the Maxwellian distributions that give minimum χ^2. The dashed lines are the modified Maxwellian distributions that give minimum χ^2.

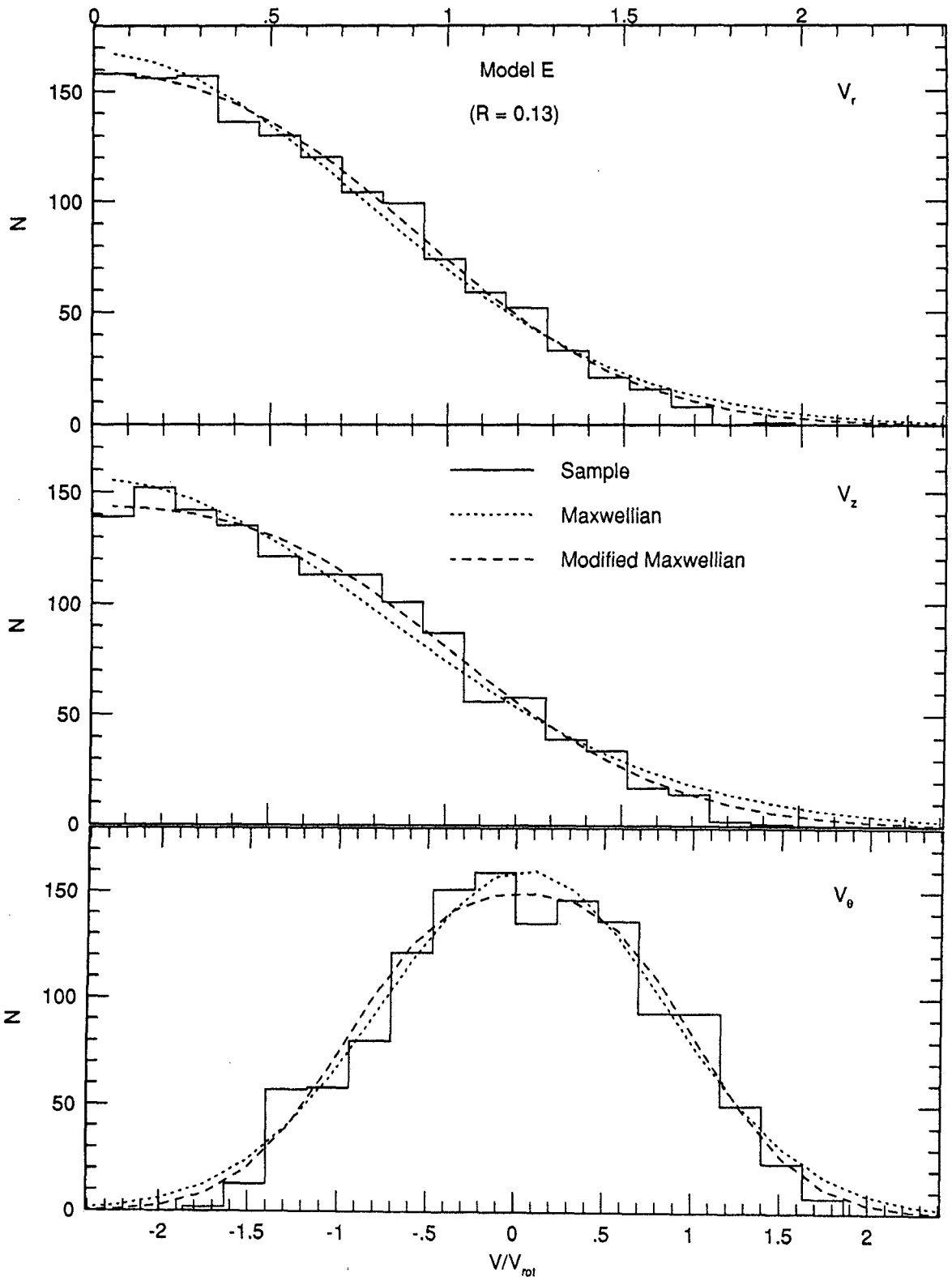

Fig. 2(c). *Velocity distributions for Model E. The horizontal axis is the velocity in the units of rotation velocity. In the panels labeled* V_θ, the horizontal axis is actually $V_\theta - \bar{V}_\theta$. The vertical axis is the number of samples and the expectation values of the Maxwellians. The solid lines are the sample distribution and the dotted lines are the Maxwellian distributions that give minimum χ^2. The dashed lines are the modified Maxwellian distributions that give minimum χ^2.

Several properties are found from figures and tables. The mean velocity and the velocity which gives minimum χ^2 in V_θ are very similar, which means that the velocity distribution is very symmetric with respect to mean velocity. The sample numbers at high velocity are much smaller than that expected from the Maxwellian distributions. This is because the initial King model has a lowered Maxwellian velocity distribution, which truncates the high velocity; there is an escape velocity due to the finite size of the system. Also, there is a smaller number of particles in the sample than in the Maxwellian distribution, near zero velocity in V_r and V_z, and near mean velocity in V_θ. The reason for this is probably that the velocities of particles are speeded up during the collapse of baryonic matter, thus causing the increase of velocity dispersion and lack of low velocity particles relative to the high velocity particles. The Maxwellian matches the overall shape of the sample distribution which fits most of intermediate regions of the velocity bins well. There are no big differences among the models. The χ^2 values in the tables show that most of the sample profiles are similar to Maxwellians. We examine the cases which have large χ^2 values. It turns out that the major contribution to χ^2 comes from the large fluctuations of one or two bins near mean velocity and one bin at the high velocity end. The large fluctuation near the mean velocity would be reduced if we had a larger number of particles. In summary, the general shape of velocity distribution is similar to a Maxwellian, but it has smaller values near mean velocity and truncated high velocity profiles.

It is often useful to provide analytic fits to better match the velocity distribution of the sample. We modified the Maxwellian distribution as follows,

$$f(V) = A\ N'(1 + cV^2) \exp\left[-\frac{V^2}{2b^2}\right], \tag{13}$$

for V_r, V_z, and

$$f(V) = A\ N'[1 + c(V - \bar{V})^2] \exp\left[-\frac{(V - \bar{V})^2}{2b^2}\right], \tag{14}$$

for V_θ, where the normalization constant is

$$A = [\sqrt{2\pi}\ b(1 + b^2 c)]^{-1}. \tag{15}$$

The results for this scheme are also shown for our Model E in Figures 2a - 2c. The values of the above constants and chi squared values are given for all our models in Table 2a - 2f of Oh (1989). This modified Maxwellian distribution gives flatter and lower distribution than that of Maxwellian at low velocity region, and also lower values in high velocity part, which is closer fitting to the sample data. This new fitting improves the chi squared value significantly in most cases. There are still unsatisfactory results in some cases, mainly because of the large fluctuations in sample distributions.

IV. SUMMARY

We found several results in our simulations:

1. We got relatively flat rotation curves, in agreement with previous results.

2. After the dissipational collapse of baryonic matter, the mean rotation velocity of dark matter in the plane of the disk is much smaller than the disk rotation velocity.

3. Dark matter particles in the plane of the disk have a roughly Maxwellian velocity distribution about the mean velocity. However there are fewer particles at high velocity and near mean velocity, compared with the best-fitting Maxwellian. But our modified Maxwellian distribution fits better.

4. The response of the halo shows no significant differences between slow collapse and fast collapse of the baryonic matter.

We assume no angular momentum transfer between baryonic matter and dark matter in our simulation, but Katz & Gunn (1991) found angular momentum transfer from baryonic matter to dark matter. The effect of angular momentum transfer will be equivalent to the simulation with higher initial λ of dark matter. But our results show that there is no significant difference between the cases of high λ and low λ. Moreover major angular momentum

transfer occurs inside 5 kpc of disk in Katz & Gunn's simulation, whereas we consider velocity distribution near solar position (7 - 9 kpc). Therefore angular momentum transfer between baryonic matter and dark matter is not likely to alter our basic conclusion.

K.S.O. was supported by fellowships from the Korean government, the University of California, Santa Cruz, and International Center for Theoretical Physics, Trieste. K.S.O acknowledges the helpful comments from G. R. Blumenthal, S. M. Faber, and J. R. Primack.

REFERENCES

Aarseth, S. J., & Fall, S. M. 1980, *Ap. J.*, **236**,43.
Aarseth, S. J. 1985, in *Multiple Time Scales*, ed. J. W. Brackhill and B. I. Cohen, (New York : Academic), p.377.
Bahcall, J. N., Schmidt, M., & Soneira, R. M. 1982, *Ap. J. (Letters)*, **258**, L23.
——-. 1983, *Ap. J.*, **265**, 730.
Bahcall, J. N., & Soneira, R. M. 1980, *Ap. J. Suppl.*, **44**, 73.
Barnes, J., & White, S. D. M. 1984, *M. N. R. A. S.*, **211**, 753.
Barnes, J., 1987, in *Nearly Normal Galaxies*, ed. S. Faber, (New York: Springer), p.154.
Barnes, J., & Efstathiou, G. 1987, *Ap. J.*, **319**, 575.
Becklin, E. E., & Neugebauer, G. 1968, *Ap. J.*, **151**, 145.
Blumenthal, G. R., Faber, S. M., Flores, R., & Primack, J. R. 1986, *Ap. J.*, **301**, 27.
Blumenthal,G. R. 1988, in *IAU Symposium 130, Large Scale Structure of the Universe*, ed. J. Audouze *et al.* (Dordrecht : Kulwer Academic Publishers), p. 421.
Bosma, A. 1978, Ph. D. Thesis, Groningen.
Caldwell, J. A. R., & Ostriker, J. P. 1981, *Ap. J.*, **251**, 61.
Casertano, S., & van Gorkom, J. H. 1991 *Astron. J.*, **101**, 1231.
de Vaucouleurs, G., 1977, *Astron. J.*, **82**, 456.
de Vaucouleurs, G., & Buta, R. 1978, *Astron. J.*, **83**, 1383.
Drukier, A., Freese, K., & Spergel, D. 1986, *Phys. Rev.*, **D33**, 3495.
Efstathiou, G., & Jones, B. J. T. 1979, *M. N. R. A. S.*, **186**, 133.
Fall, S. M., & Efstathiou, G. 1980, *M. N. R. A. S.*, **193**, 189.
Freeman, K. 1970, *Ap. J.*, **160**, 811.
Freese, K., Frieman, J., & Gould, A. 1988, *Phys. Rev.*, **D37**, 3388.
Frenk, C. S., White, S. D. M., Efstathiou, G., & Davis, M. 1985, *Nature*, **317**, 595.
Gibbons, J. D. 1976, in *Nonparametric Methods for Quantitative Analysis*, (New York : Holt, Rinehart and Winston), p. 56.
Hoffman, Y. 1988, *Ap. J.*, **328**, 489.
Katz, N, & Gunn, J. E. 1991, *AP. J.*, **377**, 365.
King, I. R. 1966, *Astron. J.*, **71**, 64.
——-. 1971, *Astr. Ap.*, **11**, 377.
Oh, K. S. 1989. Ph. D. thesis, Univ. California, Santa Cruz.
Peebles, P. J. E. 1971 *Astr. Ap.*, **11**, 377.
Primack, J. R., Seckel, D., & Sadoulet, B. 1988, *Ann. Rev. Nucl. Part. Sci.*, **38**, 751.
Quinn, P. J., Salmon, J. K., & Zurek, W.H. 1986, *Nature*, **322**, 329.
Quinn, P. J., & Zurek, W.H. 1988, *Ap. J.*, **331**, 1.
Rubin, V. C., Ford, W. K., & Thonnard, N. 1980, *Ap. J.*, **238**, 471.
——-. 1982, *ibid.*, **261**, 439.
Rubin, V. C., Burstein, D. Ford, W. K., & Thonnard, N. 1985, *Ap. J.*, **289**, 81.
Ryden, B. S., & Gunn, J. E. 1987, *Ap. J.*, **318**, 15.
Smith, P. F., & Lewin, J. D. 1990, *Phys. Rept.*, bf 187, 203.
Toomre, A. 1963, *Ap. J.*, **138**, 385.
Young, P. J. 1976, *Astron. J.*, **81**, 807.